Article

Thermal, Mechanical, and Morphological Characterisations of Graphene Nanoplatelet/Graphene Oxide/High-Hard-Segment Polyurethane Nanocomposite: A Comparative Study

Muayad Albozahid [1,*] , Haneen Zuhair Naji [2] , Zoalfokkar Kareem Alobad [3], Jacek K. Wychowaniec [4,†] and Alberto Saiani [4,*]

1   Department of Materials Engineering, Faculty of Engineering, University of Kufa, Najaf 54003, Iraq
2   Department of Chemical Engineering, Faculty of Engineering, University of Babylon, Hilla 51002, Iraq
3   Department of Polymers Engineering and Petrochemical Industries, Faculty of Materials Engineering, University of Babylon, Hilla 51002, Iraq
4   Department of Materials, Manchester Institute of Biotechnology, School of Natural Sciences, Faculty of Science and Engineering, The University of Manchester, Manchester M13 9PL, UK
*   Correspondence: moayad.zahid@uokufa.edu.iq (M.A.); a.saiani@manchester.ac.uk (A.S.); Tel.: +964-7719097006 (M.A.)
†   Current address: AO Research Institute Davos, Clavadelerstrasse 8, 7270 Davos, Switzerland.

Abstract: The current work investigates the effect of the addition of graphene nanoplatelets (GNPs) and graphene oxide (GO) to high hard-segment polyurethane (75% HS) on its thermal, morphological, and mechanical properties. Polyurethane (PU) and its nanocomposites were prepared with different ratios of GNP and GO (0.25, 0.5, and 0.75 wt.%). A thermal stability analysis demonstrated an enhancement in the thermal stability of PU with GNP and GO incorporated compared to pure PU. Differential Scanning Calorimetry (DSC) showed that both GNP and GO act as heterogeneous nucleation agents within a PU matrix, leading to an increase in the crystallinity of PU. The uniform dispersion and distribution of GNP and GO flakes in the PU matrix were confirmed by SEM and TEM. In terms of the mechanical properties of the PU nanocomposites, it was found that the interaction between PU and GO was better than that of GNP due to the functional groups on the GO's surface. This leads to a significant increase in tensile strength for 0.5 wt.% GNP and GO compared with pure PU. This can be attributed to interfacial interaction between the GO and PU chains, resulting in an improvement in stress transferring from the matrix to the filler and vice versa. This work sheds light on the understanding of the interactions between graphene-based fillers and their influence on the mechanical properties of PU nanocomposites.

Keywords: high hard-segment polyurethane; graphene nanoplatelets; graphene oxide; nanocomposites; thermal stability; mechanical properties

1. Introduction

It is critical to design high-performance polymer nanocomposites by achieving a uniform dispersion of nanofillers and strong interfacial adhesion between nanofillers and polymer matrices in nanocomposite systems [1–3]. Recently, many researchers have focussed their attention on the use of various types of nanofillers such as graphene, carbon nanotubes, and nanoclays, among others [4–6]. Nanocomposites' performance depends on the substantial features of the nanofiller (the geometrical dimensions, surface area, aspect ratio, etc.) and the dispersion/distribution state of the nanofiller, as well as nanofiller–nanofiller and nanofiller–polymer interactions [5,7]. Poor dispersion and weak interfacial bonding still pose a challenge in the design of effective carbon nanofiller–polymer matrix nanocomposites [8].

Polyurethanes (PUs) are semicrystalline copolymers consisting of alternating hard and soft segments [9–12]. Most PUs are formed from polyether/polyester polyols along with

aliphatic or aromatic di-isocyanates [6,13,14]. Indeed, a phase-separated microstructure is formed in PUs due to the thermodynamic incompatibility between hard segments and soft segments, providing a unique and outstanding mechanical performance [12]. A suitable choice of raw chemicals and dispersion methods leads to improved mechanical, thermal, and electrical properties [3,13]. Polyurethane (PU) has various applications, including fibres, coatings, adhesives, and smart actuators [7,15–18].

Graphene is a two-dimensional sheet with a two-dimensional honeycomb arrangement of carbon atoms [19]. Graphene and its derivatives are considered promising nanofillers for high-performance polymeric nanocomposite materials due to their unique mechanical, rheological, thermal, and electrical properties [2,20–22]. In fact, graphene usage has increasingly grown in different industrial applications over the past decade [23]. In particular, graphene nanoplatelets (GNPs) are often used as nanofillers, consisting of a few layers of graphene sheets [24]. Graphene oxide (GO) has also been considered one of the most promising multifunctional fillers derived from graphene [25]. The production of GO leads to oxygenated (hydroxyl, epoxide, and carboxyl groups) defects in its lattice [18,26,27], which affect the final properties of GO.

Interfacial interactions between nanofillers and polymer chains can provide a feasible way to build high-performance polymer nanocomposites [3,4,7]. Dispersion approaches can basically be classified into three methods: (i) melt blending, (ii) solution mixing, and (iii) in situ polymerisation [3,28]. The degree of dispersion between these methods can be varied and depends on the exact physicochemical interactions between the polymer and the nanofillers [29].

The intermolecular interactions during this process can lead to the restacking of 2D nanomaterials driven by the Van der Waals interactions when at close proximity [30]. For instance, high shear stress during melt mixing was reported to be inadequate for overcoming the agglomeration of nanofillers during mixing [31]. Consequently, in situ polymerisation can be a better choice for the high dispersion of nanofillers [26,32].

There are a significant number of studies devoted to the use of GNP, GO, or both to reinforce various kinds of polyurethane [26,33–35]. The reinforcements have shown improved electrical conductivity, mechanical properties, and thermal properties compared to pure PUs [36,37]. Graphene and GO are both advanced carbon nanomaterials that have a high mechanical strength and can be easily functionalised to tune interactions with polymers. Based on the authors' knowledge, the dispersion and interaction of these nanofillers in polymer matrices could effectively improve crucial properties such as the mechanical and thermal properties of different polymers [38]. There is currently a lack of studies on this type of polyurethane with two types of nanoscale fillers with different functional groups on their surfaces. As such, the main objective of the current study is to obtain and characterise new hard-segment polyurethane nanocomposites with a new type of chain extender, 1,5 pentanediol, and using two kinds of nanoscale additives with different functional groups: GNP and GO.

2. Experimental Method

2.1. Materials

Graphene nanoplatelets (GNP), with an average thickness of 6–8 nm and a typical surface area of 120 to 150 m^2/g, were purchased from Lansing, MI, USA (XG sciences.com). Polyurethane was produced according to a two-step polymerisation process using polyether polyol as a soft segment purchased from Sigma-Aldrich, UK, with functionality of 2.0 and an average molecular number M_n = 2000 g/mol. The chain extender (1,5-Pentanediol) and isocyanate, MDI (4,4' methylenebis phenyl isocyanate), which represent the hard segments, were purchased from Sigma-Aldrich, UK. A catalyst (DABCO-S) and the solvent N,N dimethylene-acetamide (DMAC) were utilized to complete production of the PU.

2.2. Preparation of Graphene Nanoplatelets (GNP)

GNP powder (wt.%) was dispersed with DMAC solvent before mixing with PU at a concentration of 2 mg/mL. A sonication bath method (frequency = 37 KHz) was utilised for dispersion for half an hour to prevent GNP aggregation/stacking during the in situ polymerisation process.

2.3. Preparation of Graphene Oxide (GO)

Graphene oxide (GO) was prepared using a modified Hummers' method [39]. Briefly, 5 g of natural flake graphite (Graphite Trading Company) and $NaNO_3$ (3.75 g) were continuously stirred in concentrated sulphuric acid (170 mL). The mixture was then cooled and kept in an ice bath for 2 h with stirring to maintain a very low temperature of 2 °C. Afterwards, $KMnO_4$ (25 g) was gradually added over 60 min with constant stirring and, to avoid a sudden increase in temperature, the rate of addition was carefully controlled. Then, the mixture was removed from the ice bath and allowed to warm to room temperature and left stirring for 7 days. The mixture became thicker and brownish over time. Then, the dark mixture was gradually dispersed into 550 mL of water with 15 mL (5 wt.%) of H_2SO_4 for approximately 1 h. Over 5 min, 10 mL of hydrogen peroxide (30 vol. %) was added with considerable effervescence; the mixture converted into a yellow/gold glittery suspension and was stirred for a further 2 h. After that, the mixture was additionally diluted with 500 mL of H_2O containing 9 mL (3 wt.%) of H_2SO_4 and 2 mL (0.5 wt.%) of H_2O_2, and left stirring overnight. Finally, the subsequent addition of water continued until the pH of the GO solution reached neutral (pH = 7).

2.4. Dispersion Techniques

PU nanocomposites were prepared using different dispersion methods in order to obtain better dispersion quality and an improvement in their physical properties [40]. The final product of synthesis was a solution-based PU with a high amount of DMAC solvent incorporated with GNP and GO by different dispersion techniques. Both GNP and GO were dispersed in DMAC using a sonication bath and magnetic stirring before being added to the PU during the synthesis process to ensure better quality dispersion. It was found that a sonication bath (power = 80 W; frequency = 37 kHz) of these carbon additives can exhibit a high degree of exfoliation compared to a magnetic stirrer (overnight). The difference between the sonicated and magnetic stirring-treated (GO and GNP) nanofillers is shown via the images in Figure 1.
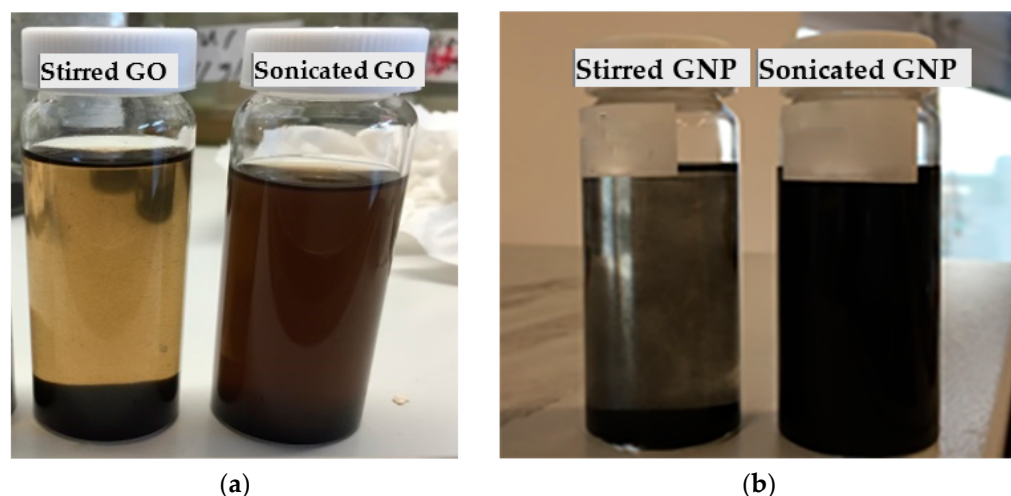

| (a) | (b) |

Figure 1. Dispersibility behaviour of GNP and GO in DMAC solvent (0.5 mg/mL) after ultrasonication and magnetic stirring-processes and being left for 24 h: (**a**) GO (**b**) GNP.

2.5. Preparation of PU/GNP and PU/GO Nanocomposites

A two-step polymerisation approach was carried out to synthesise the PU matrix, as reported in our previous study [21], with a hard-segment ratio of 75% HS. The in situ polymerisation approach was used for the preparation of PU/GNP and PU/GO nanocomposites with a weight fraction value, for example, of 0.25 g of GNP/GO, added to 100 g of an exact amount of PU polymer for a ratio of 0.25 wt.%, and so on, since the GNP/GO solution was combined with the chain extender in the second stage. After completing the synthesis process, the PU/GNP and PU/GO solutions were dried in a furnace at 80 °C for three days. The test samples of both PU/GNP and PU/GO nanocomposite materials were performed by an injection-moulding process using a Haake Minijet II (Thermo Scientific, Waltham, MA, USA) with a barrel temperature of 200 °C, mould temperature of 50 °C, injection pressure at 850–1100 bar for 10 s, and holding pressure at 400 bar for 5 s. The synthesis process is shown in Figure 2.
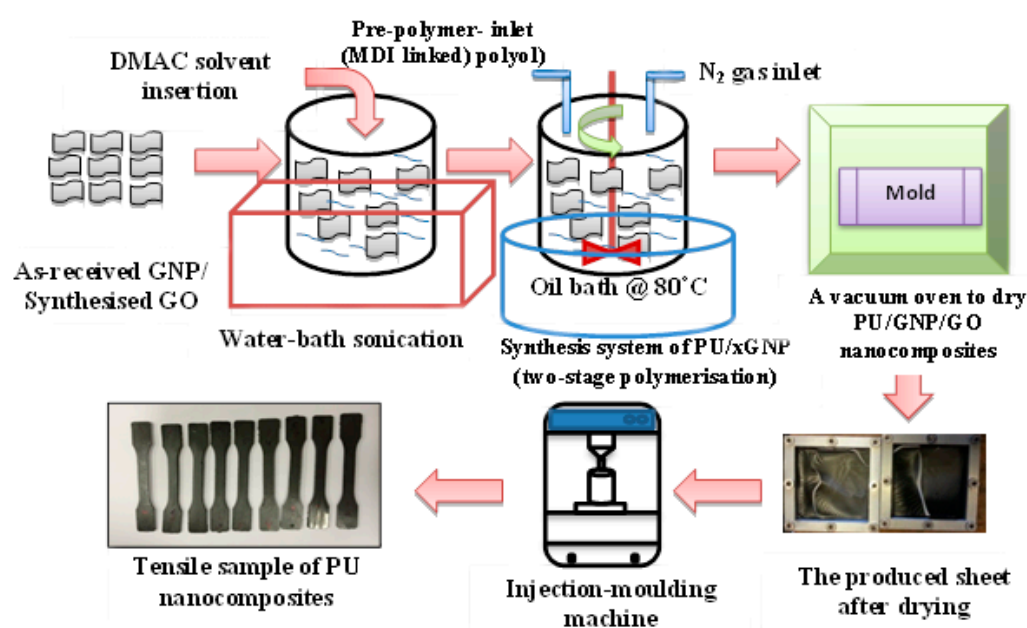

Figure 2. Schematic representation of fabrication process of PU/GNP and PU/GO nanocomposites using a sonication bath and in situ polymerisation system with an oven and nitrogen inlet to maintain the inert atmosphere environment inside the reaction vessel.

2.6. Characterisation and Measurements

2.6.1. Thermogravimetric Analysis (TGA)

TGA experiments were performed using a Q-500 (TA Instruments) under nitrogen atmosphere. A weight of samples of about 5 mg was used to measure the thermal stability of PU/GNP and PU/GO nanocomposites via their heating to 700 °C at a heating rate of 10 °C/min.

2.6.2. Differential Scanning Calorimetric Analysis (DSC)

Q100 (TA Instruments) was used to investigate the thermal properties of PU/GNP nanocomposites using an auto-sampler and the Indium Calibration Standard. The samples weighed about 7–11 mg, and the custom protocol that was applied consisted of a cool/heat/cool/heat sequence with a heating range of −90 °C to 200 °C and a rate of 10 °C/min in an N_2 atmosphere.

2.6.3. X-ray Diffraction (XRD)

For X-ray diffraction (XRD), an X'Pert X-ray diffractometer was utilized together with a Cu Kα radiation source (λ = 1.542 Å) to first identify the GNP and GO structures in a powder form. The crystallinity plane degree of semicrystalline PU/GNP and PU/GO nanocomposites was attained as well that for injection-moulded samples with a rectangular shape of 1 mm $\times$ 0.5 mm.

2.6.4. Small-Angle X-ray Scattering (SAXS)

SAXS experiments were carried out on Beamline I22 at the Diamond Light Source (DLS) facility in Didcot, UK. The beam's energy was 12.4 keV, equivalent to an X-ray wavelength of 0.1 nm. Samples were suspended on a metal grid using Kapton tape. Acquisition time varied from 1 to 0.01 s depending on the scattering intensity of the sample; the pixel array detector used to collect the SAXS data was the Pilatus P3-2M (from Dectris). There was a 3.47 m fixed distance between samples and the detector, resulting in a momentum transfer vector range of 0.05 (nm^{-1}) < q = (4π/λ)sin(θ/2) < 3.0 (nm^{-1}), where θ is the scattering angle and λ the wavelength of incident photons. Calibration of the momentum transfer was performed using silver behenate powder. Air was applied as background and was subtracted from all measurements, while the subtraction mask was formed using glassy carbon. Data were reduced using the processing tools in the DawnDiamond software suite. The 2D scattering photon patterns were integrated using an azimuthal integration tool to obtain 1D scattering patterns. As a result of the irregular structures of semi-crystalline materials such as PUs, SAXS can provide a scattering signal with different homogeneities at a typical length scale (d-spacing). This is calculated using Bragg's law: $d_m = 2\pi/q^*$, where q^* is the maximum of the scattering peak. Based on Bragg's law, the degree of phase separation of multi-block copolymers can be predicted from a one-dimensional scattering pattern for most quantitative analysis; the phase structure can be obtained from the position of the peak of a q scale. This q vector can yield the correlation length between two different phases.

2.6.5. Transmission Electron Microscopy (TEM)

The morphological features of PU/GNP and PU/GO were investigated via a transmission electron microscope (Philips CM200, 200 kV, Tokyo, Japan). For TEM measurement, the PU/GNP and PU/GO samples were prepared via cutting sample into slices approximately 50–60 nm in thickness, which were cut from the core of the samples using a diamond blade knife and an ultra-microtome machine (Leica EM UC6). Samples were deposited on square mesh copper TEM grids (300 Mesh)—purchased from Agar Scientific (UK)—in the distilled water solution.

2.6.6. Scanning Electron Microscopy (SEM)

The morphological features of PU/GNP and PU/GO nanocomposites were detected using field-emission SEM (FESEM-CXL30). The cryogenically fractured surface of the nanocomposites was coated with a thin film of gold in order to make it conductive with respect to the incident electron beam, thus producing a better SEM image. This process was conducted using a rotary-pumped coater (Q150R Plus from Quorum (Lewes, UK)).

2.6.7. Mechanical Test

The tensile properties of the pure PU and PU/GNP and PU/GO nanocomposites were tested using a universal testing machine (type an Instron 1122). All samples were tested under specific conditions (humidity ~50%, with a temperature ~25 °C) within a controlled room. The dumbbell-shaped test specimens were made by injection moulding machine according to the ISO 527-2 1BA standard. The samples were kept overnight before testing; the tensile test was performed with crosshead speed of 10 mm/min for at least 5–7 samples.

3. Results and Discussion

3.1. Characterisation of Structure and Morphology of GNP/GO

3.1.1. SEM and TEM Analysis

The TEM and SEM techniques were used to investigate the structure and morphology of the GO and GNP nanofillers. Figure 3 shows the SEM and TEM images for both GO and GNP. The SEM images of GO show aggregation and folded regions (indicated by red arrows in Figure 3a) due to oxidation and restacking processes, leading to the formation of a crumpled and fluffy structure [41]. In contrast to GO, both the SEM and TEM images of the GNP reveal folded, rolled up, and overlapping GNP flakes. It is well known that sonication energy can trigger the folding of GO/GNP flakes, which restack after sonication [11,12]. This outcome is attributed to the effect of Van der Waals forces on graphene sheets, leading to restacking and disordered, aggregated regions in the graphene derivatives [42]. Figure 3d illustrates the TEM images of GO at a nano-size thickness and a small scale, which also indicates the folded regions besides the wrinkled regions owing to the effect of the chemical treatment.
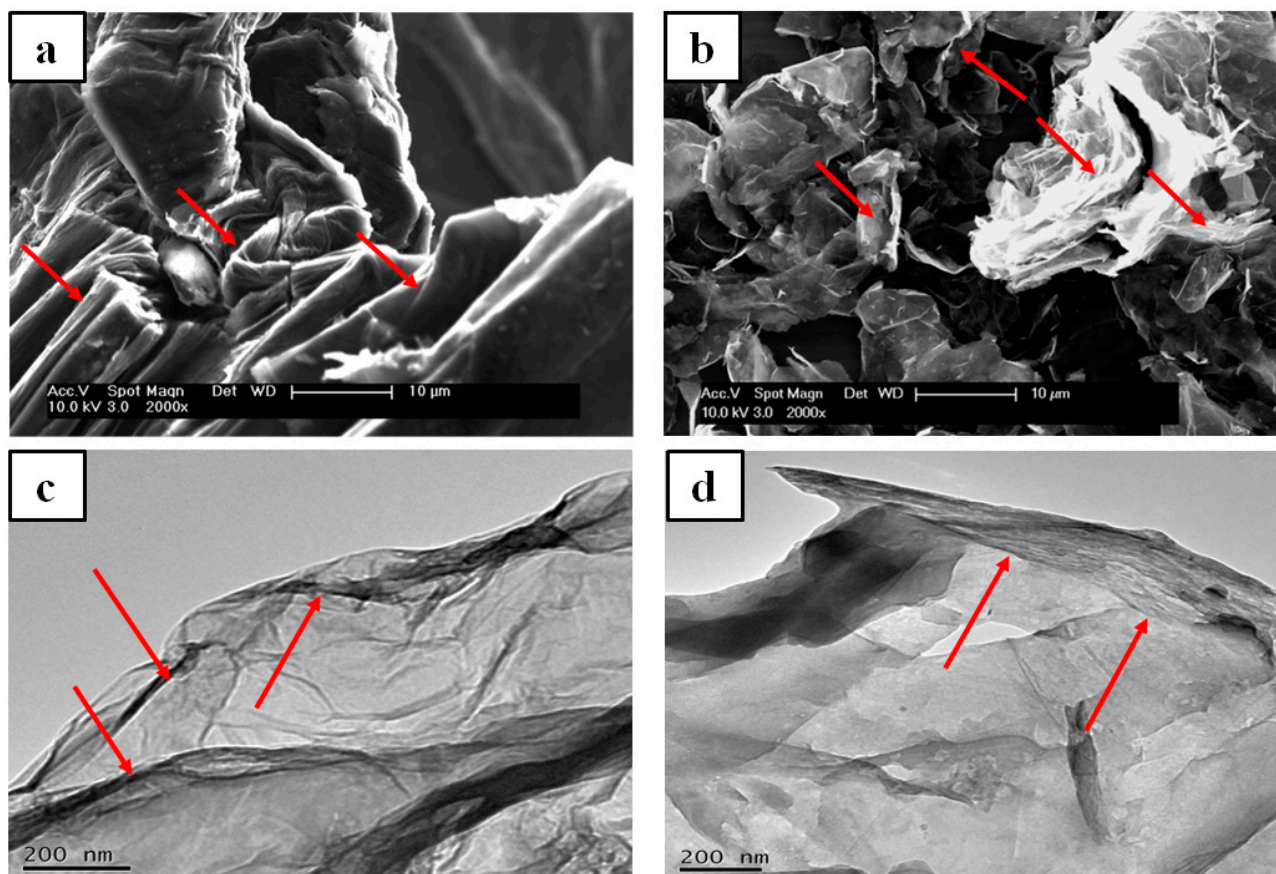

Figure 3. SEM and TEM images: (**a**,**c**)—GO; (**b**,**d**)—GNP. The red arrows indicate the folding and wrinkling areas and aggregation regions of GO.

3.1.2. XRD Results

Figure 4 presents the XRD diffraction pattern of GNP and GO compared with pure graphite. It is well known that the XRD test is usually used to investigate the crystal structures of different materials and determine their interlayer spacing (d) using Bragg's equation, where distance (d) relates to the beam-diffraction angles of an incident X-ray line. The XRD diffraction pattern of the as-received GNP exhibits two peaks located at 26.52° and 54.62°, corresponding to Bragg's reflection planes 002 and 004 and interlayer d-spacing of 3.35 Å and 1.68 Å, respectively [18,43]. As expected from previous studies [43,44], both peaks of the GNPs indexed to pure graphite, which indicates the ability of the as-received

GNPs to maintain the crystalline structure of graphite [44,45]. Yet, after oxidation, the highest diffraction peak of graphite shifted to 10.82°, which indicates the effect of the presence of oxygen within the interlayer spaces of graphite [46]. The effect of oxygen functional groups such as carbonyl, hydroxyl, carboxyl, and epoxy groups in GO and some structural defects cause the increase in d-spacing of the highest peak of graphite from 3.35 Å to 8.18 Å, as reported in previous studies [47].
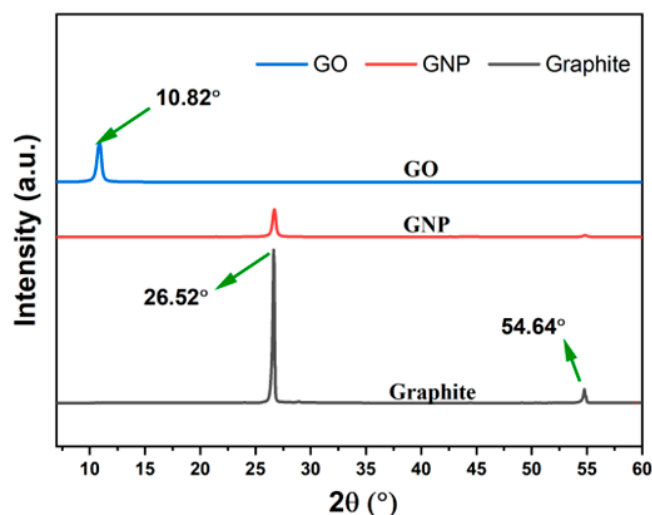

Figure 4. XRD pattern of GNPs and GO in comparison with pure graphite.

3.2. TGA Results

All the gravimetric measurements of pure PU and its nanocomposites with GNP and GO are shown in Figure 5. Figure 5a,c display the normal TGA curves of the PU, PU/GNP, and PU/GO nanocomposites with various weight percentages. The weight loss is plotted with a temperature range from 0 °C to 700 °C. It can be seen that thermal degradation of the polymers can be divided into three steps: the complete degradation of the main chains, the rupture of the side chains with volatile products, and the formation of char residues [48,49]. It was observed that the onset temperature (T_{onset}) of pure PU started increasing after the addition of GNPs and GO, and thus both the PU/GNP and PU/GO samples showed a similar trend of thermal stability enhancement, even at a low nanofiller loading. Such a difference in the improvement of the thermal stabilities of the PU nanocomposites via the addition of GNPs and GO is related to the high thermal stability of GNPs compared to GO [50–52]. The TGA results can provide evidence of the quality of the nanofillers that are linked with the polymer. Overall, all the PU filled with GNPs and GO exhibited higher thermal stability performance than that of pure PU. The maximum rate of degradation temperature (T_{max}) of PU and its nanocomposites as obtained from a DTG thermogram are summarised in Table 1. The DTG curves of PU and its nanocomposites (see Figure 5c,d) consist of a two-stage mechanism of thermal degradation. Firstly, the dissociation of the urethane linkage of PU occurs, converting the urethane groups to isocyanate and alcohol. Secondly, the degradation is associated with the mass loss of the soft segments [18,53].

The findings suggest that PU is thermally stable around 300 °C, while hard segments start to degrade after temperatures in the range of 330 °C–340 °C. The soft segments start to degrade afterwards, with a maximum temperature of 370 °C. The addition of GNP and GO gradually increases the onset temperature by 8 °C and the T_{max} of the DTG results by 10 °C with minimum GNP and GO incorporation. The improved thermal stability results from the maximising of the physico-chemical properties due to the incorporation of nanofillers, since the barrier effect of PU filled with GNP and GO might be more effective in preventing the emission of degraded products, thus yielding high barrier performance [54–57]. As a result, this tortuous effect prevented the escape of all of the gases generated during the heating process and released from the PU/GNP and PU/GO samples [22,58,59].
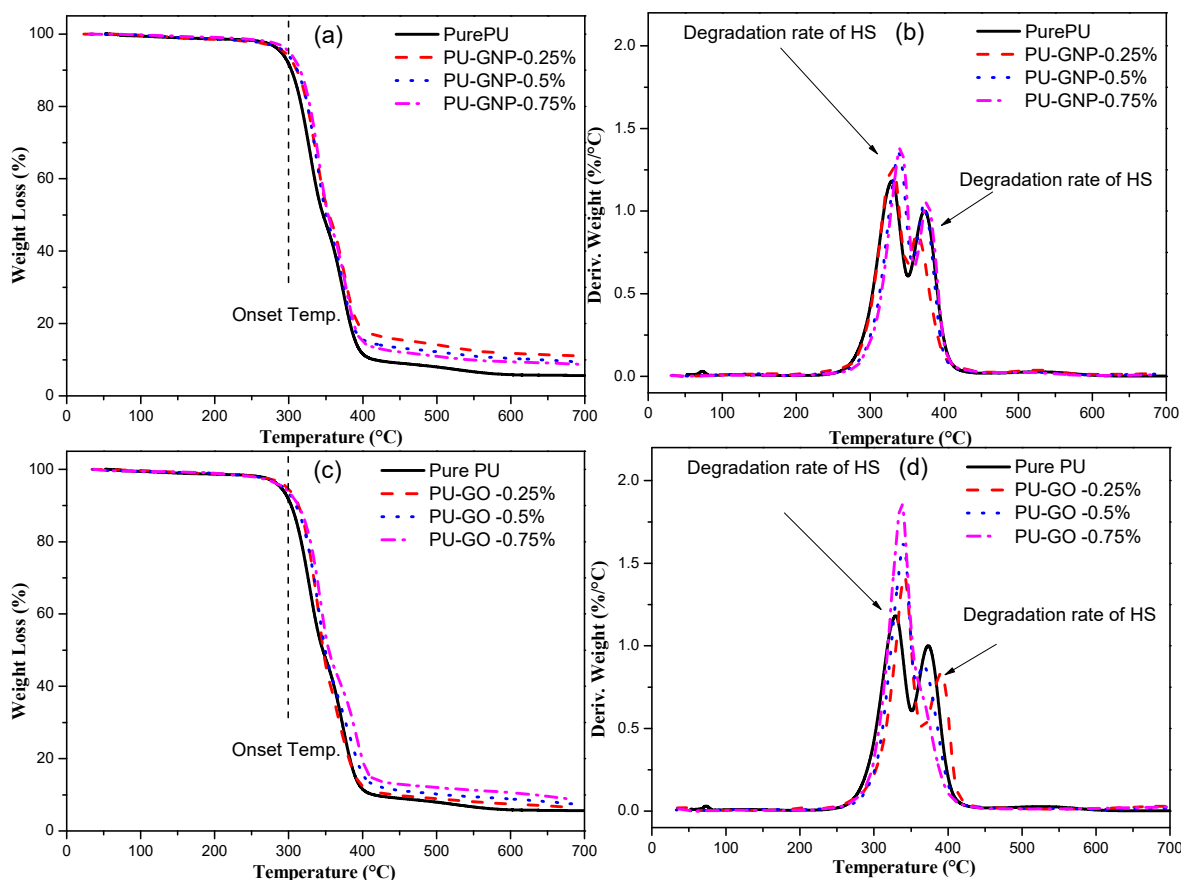
Figure 5. TGA curves (10 °C/min) of PU/GNP nanocomposites and PU/GO nanocomposites compared to pure PU: (**a**) TGA curves; (**b**) DTG curves.with GNP nanofiller, (**c**) TGA curves; (**d**) DTG curves, with GO nanofiller.

Table 1. TGA data for GNP- and GO-filled PU.

	TGA				DTG							
	$T_{Onset} \pm SD$		Residual Mass (%)@600 °C $\pm$ SD		1st Step (HS Degradation)				2nd Step (SS Degradation)			
					T_{max} (°C) $\pm$ SD		Dev. Mass (%/°C) $\pm$ SD		T_{max} (°C) $\pm$ SD		Dev. Mass (%/°C) $\pm$ SD	
	GNP	GO	GNP	GO	GNP	GO	GNP	GO	GNP	GO	GNP	GO
Neat PU	297.76 ± 1.10	297.76 ± 1.10	8.50 ± 2.88	8.50 ± 2.88	333.70 ± 1.34	333.70 ± 1.34	1.16 ± 0.13	1.16 ± 0.10	369.00 ± 2.45	369.00 ± 2.45	0.83 ± 0.11	0.83 ± 0.11
PU + 0.25 (wt.%)	308.7 ± 3.73	307.67 ± 3.80	10.11 ± 0.03	6.76 ± 1.30	334.80 ± 2.51	342.14 ± 1.80	1.24 ± 0.03	1.50 ± 0.05	368.20 ± 4.01	380.80 ± 1.40	0.92 ± 0.09	0.95 ± 0.02
PU + 0.5 (wt.%)	309.20 ± 4.34	308.90 ± 1.50	10.5 ± 1.13	7.79 ± 0.87	338.67 ± 1.40	343.57 ± 2.40	1.38 ± 0.11	1.8.80 ± 0.10	372.86 ± 3.30	382.88 ± 2.70	0.99 ± 0.03	1.1 ± 0.65
PU + 0.75 (wt.%)	314.56 ± 0.55	315.46 ± 2.30	9.62 ± 1.62	10.50 ± 0.27	341.47 ± 2.02	343.6 ± 2.70	1.41 ± 0.12	1.34 ± 2.8	375.80 ± 2.02	392.45 ± 2.49	1.02 ± 0.05	1.30 ± 0.77

3.2.1. DSC Results

DSC was carried out in order to further study the thermal behaviour, including the melting temperature (T_m), crystallisation temperature (T_c), melting enthalpies (ΔH_m), and crystallisation enthalpies (ΔH_C) of PU and its nanocomposites. Thermal transition variations were investigated by the incorporation of GNP and GO using DSC thermograms, as summarised in Table 2. DSC can provide evidence of the crystal structure of hard segments through the change in the thermal behaviour of the PU/GNP and PU/GO nanocomposites in comparison with neat PU. The DSC scans were conducted with PU nanocomposites containing GNP/GO at different weight loadings (0.25, 0.5, and 0.75 wt.%). The results show that multi-endotherms of the melting temperatures can be detected

within semi-crystalline PU. For example, the first heating scan reveals that the endothermic peaks relevant to the melting temperature (T_m) occurred at around 171 °C for pure PU and then increased to 174 °C and 183 °C for PU containing GNP and GO at 0.75 wt.%. However, the first heating scan illustrates several variations between the first and second heating scan due to the thermal history [60,61]. The second heating scan appears to be more precise compared to the first scan, as the manufacturing parameters varied during the production process owing to the absence of the thermal history [14,48,49]. Thus, an improvement in the PU nanocomposites can be seen in the presence of GNP and GO [7]. The enthalpy of fusion of the second heating scan was observed to increase with the GNP loading (ΔH_m rose from 25.44 J/g to 26.4, 27.1, and 29 for loadings of 0.25, 0.5, and 0.75%, respectively). This increase in such an endothermic transition could be attributed to the restricted mobility of the PU chains in the presence of nanofillers [26,62]. It is hard to obtain the glass transition temperature (T_g) of hard segments due to their mixing with the melted soft segments despite the low ratio of the last one. The presence of multiple peaks in the DSC analysis could refer to several melting–crystallisation processes of the originally formed long-ordered/short-ordered structures of the predominant phase (hard phase) [62,63]. The maximum enhancement in terms of the T_m was seen for higher loadings (0.75 wt.%) of both GNP and GO. Furthermore, the crystallisation process was accelerated for the hard segment of PU and was significantly affected by the uniform dispersal of the GNP and GO nanofillers. Since the nanofillers could act as a heterogeneous nucleation agent and thus triggered the better crystallisation of the hard segments of the PU matrix [58], it was found that the T_c of the hard domains was greatest and enhanced to almost 120.4 °C and 177.61 °C at loadings of 0.75 wt.% of GNP and GO within the PU matrix, respectively, from approximately 118 °C of pure PU. These findings can be attributed to the larger size of GO and the oxygen-rich functionalities in its structure; therefore, it can act as a positive heterogeneous agent to a greater extent than GNP and cause the HS to improve its intrinsic crystallization within the PU matrix [14]. Meanwhile, the crystallisation enthalpy of the nanocomposites with GO is lower than those with GNP due to the heterogeneous nucleation effect as interpreted in the previous sentence. Similar results regarding DSC were found in recent studies [52,58].

Table 2. Thermal transitions of PU/GNP and PU/GO nanocomposites compared to pure PU.

	First Heating				First Cooling				Second Heating			
	GNP		GO		GNP		GO		GNP		GO	
	$T_m \pm$ SD	$\Delta H_m \pm$ SD	$T_m \pm$ SD	$\Delta H_m \pm$ SD	$T_c \pm$ SD	$\Delta H_c \pm$ SD	$T_c \pm$ SD	$\Delta H_c \pm$ SD	$T_m \pm$ SD	$\Delta H_m \pm$ SD	$T_m \pm$ SD	$\Delta H_m \pm$ SD
Pure PU (65% HS)	171.60 ± 1.85	25.44 ± 1.39	-	-	118.31 ± 1.54	27.49 ± 0.09	-	-	174.29 ± 1.62	26.11 ± 0.07	-	-
PU + 0.25 (wt.%)	172.3 ± 0.60	26.39 ± 2.2	183.78 ± 2.77	27.59 ± 2.02	121.01 ± 1.40	28.195 ± 1.60	175.53 ± 2.60	23.07 ± 1.00	177.43 ± 0.60	25.06 ± 2.70	176.71 ± 3.10	-
PU + 0. 50 (wt.%)	172.60 ± 1.65	27.13 ± 1.34	183.73 ± 0.00	29.67 ± 1.33	120.20 ± 1.30	30.89 ± 0.67	176.62 ±1.90	25.61 ± 1.50	175.62 ± 0.67	26.13 ± 1.40	178.94 ± 2.00	-
PU + 0.75 (wt.%)	174.34 ± 1.00	26.80 ± 1.20	183.21 ± 3.05	29.13 ± 0.90	120.70 ± 2.70	33.10 ± 1.30	177.61 ± 0.00	29.87 ± 0.60	176.90 ± 0.90	26.78 ± 0.60	179.55 ± 2.60	-

The degree of crystallinity of neat PU and its nanocomposites can be calculated using the following equation:

$$X_C\% = \frac{\Delta H_m}{\Delta H_{m0}(1 - \varnothing)} \times 100 \tag{1}$$

where ΔH_m = the heat of fusion of the neat TPU-70 HS and its nanocomposites; ΔH_{m0} = the heat of fusion for the 100% crystalline TPU, which is recorded as 172.2 J/g and is in accordance with a previous study [64]; and finally, $\varnothing$ = the nanoparticle fraction in the TPU structure [64].

Thus, through this equation, the degree of crystallinity of pure PU is about 14.7%, which increased to reach 25.7% and 23.6% for the PU nanocomposites incorporated with 0.75 wt.% of GNP and GO, respectively. Even though the PU/GO nanocomposites recorded

a higher Tc in comparison with GNP, its degree of crystallinity was slightly lower than that of the PU/GNP nanocomposites at the same 0.75 wt.% loading. This can be assigned to the higher surface area of GO and the presence of oxygen functionality in its structure, leading to an increase in ΔHm and then a decrease in Xc according to the above equation [65,66]

3.2.2. Wide-Angle X-ray Diffraction (WAXS) Results

The wide-angle X-ray diffraction detected the long-range order and regularity of the PU chains, particularly the hard-segment chains, as illustrated in Figure 6. The X-ray diffractograms of the PU structure display two main diffraction peaks at 2θ values of 11° and 2θ values of 20°. The first corresponds to the interlayer spacing of the hard segments of 0.8 nm and 0.43 nm, based on Bragg's equation [61,67]. The main diffraction peaks of PU represent the long order or even the crystallinity of hard segments. With the addition of a small amount of GNPs or GO, the disappearance of the diffraction peaks of GNP and GO indicate the better exfoliation of the GNP and GO within the PU matrix due to proper dispersion [68,69]. The decrease in the intensity among the GO nanofillers is due to the oxidation process during manufacturing [12,70]. The soft segments in this study did not exhibit any diffraction peaks due to the difficulty of crystallising the polyether polyol. The diffraction of the PU/GNP nanocomposites is clearly observed when adding GNP at various loadings. On the contrary, the PU/GO nanocomposites showed relatively wide diffraction peaks, which indicate the disruption of the long-range order of hard segments and thus a reduction in the crystallinity of PU [71]. In general, the intensity of the diffraction peaks was seen to increase with an increase in the nanofiller (GNP and GO) loading. However, the diffraction peaks vanished in the case of GO incorporation, which is attributed to the presence of functional groups on the surface of GO that might have reacted with the PU chains (hard segments). Similar results to those presented in this work can also be found in previous reports on similar nanofillers [72,73].
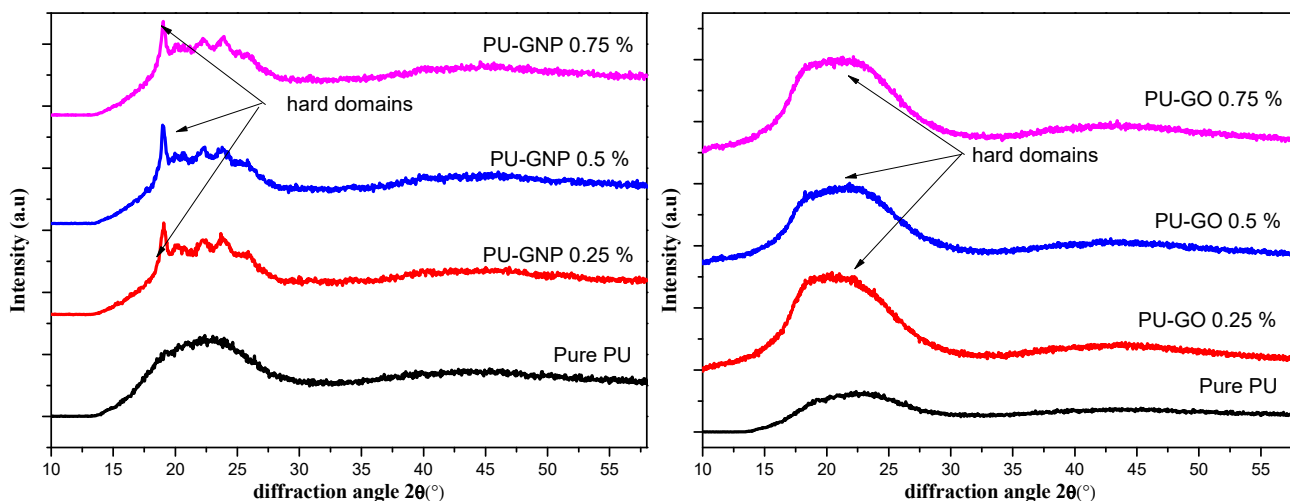

Figure 6. Semi-log plot of Y-axis of wide-angle X-ray-scattering intensity for PU/GNP/GO nanocomposites.

3.3. SAXS Results

The SAXS pattern of pure PU and its nanocomposites with GNP and GO at different concentrations (0.25 wt.%, 0.5 wt.%, and 0.75 wt.%) is shown in Figure 7. The maximum of the scattering peak (q*) of the microphase-separated pattern is observed in the scattering curve (I(q) vs. q)) [63,74]. SAXS showed a maximum scattering for all the PU samples at the same momentum transfer, q, value, as previously mentioned in a study by Saiani et al. [75]. From SAXS, the phase structure of PU was estimated to be within the length range of 1–100 nm based on the contrast between the electron densities of hard segments and soft segments. Thus, a heterogeneous microstructure of PU was produced, since the scattering intensity was directly proportional to the electron variations (Q_{inv}) (microphase separation

index) that represented the two-phase system. This could be an indicator of how hard segment interaction/association works to produce the domain size and thus the micro-phase separation of PU [74–76].
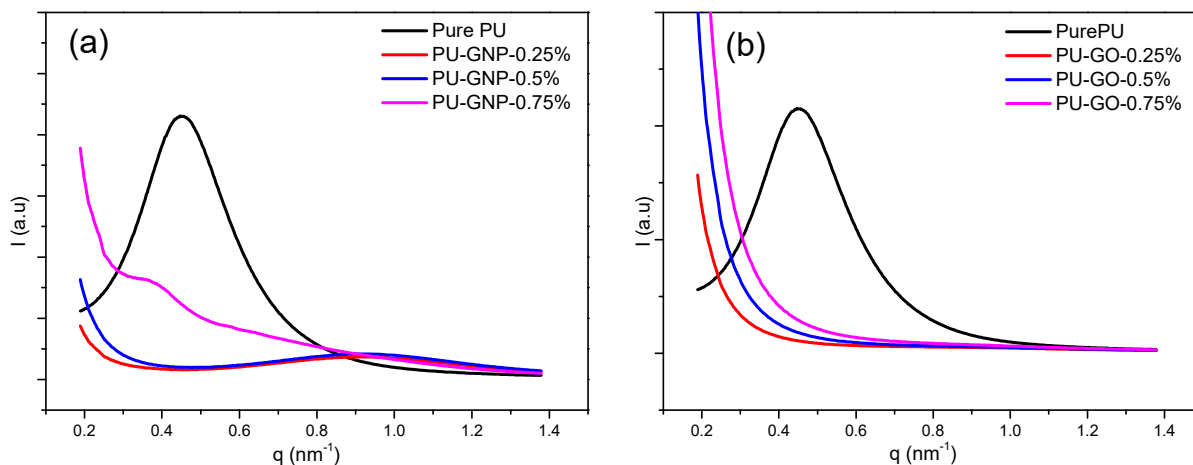

Figure 7. Semi-log plot of scattered intensity from SAXS experiments for pure PU and PU/GNP and PU/GO nanocomposites, (**a**) SAXS curves of GNP nanofiller; (**b**) SAXS curves of GO nanofiller.

In the present study, a characteristic scattering peak is observed for all the PU/GNP samples, implying the presence of a microphase-separated structure. The broadening of the peaks toward higher q values can prove the assumption of a reduction in inter-domain spacing and thus the conclusion that a better phase separation of PU has been induced by the GNPs' incorporation [63]. This assumption has been proposed previously by Teheran et al. [77]. On the other hand, a similar trend was also observed in the PU/GO nanocomposites with a partial disappearance of the scattering peak, implying that hard segments tend to be packed in a uniform pattern promoted by strong interactions with the uniformly dispersed GO [12,63,77]. In Figure 7a, the characteristic peak for pure PU is found at $q = 0.45$ nm^{-1} and that for PU/GNP with loadings of 0.25, 0.50 and 0.75 wt.% is found at $q = 1.1$ and 0.4 nm^{-1}, which corresponds to the d-spacing of pure PU and PU/GO of 13.95, 6.28, 6.28, and 15.7 nm. This current finding is in agreement with the previous XRD results. Conversely, in Figure 7b, a broad peak associated with the characteristic peak of PU/GO appears, showing no peaks for all concentrations. The disappearance of the peak indicates that there is a clear level of dispersion and interaction of GO particles in the polyurethane matrices during high-shear mixing [78]. This phenomenon is based on func-tional groups on the edge of GO that cause physical and/or chemical interactions between –OH groups in the nanoparticles and carbonyl groups in the polyurethane structures [71,79]. This contributed to the phase separation dropping between HS and SS [78]. Overall, the PU/GNP nanocomposites show a slight shift in the q_{max} towards a higher q value at low loadings, demonstrating a less interfacial interdomain region.

3.4. SEM Results

It is important to investigate the influence of the GNP and GO nanofillers' addition on the structural pattern of the PU matrix. The influence of nanofillers depends on how effectively they are dispersed in the PU matrix. A poor dispersion or distribution of GNP and GO can have a significant impact on the PU's morphology, leading to an inconsistent behaviour. Figure 8 shows a comparison of the SEM images of the cryo-fractured surfaces of the PU/GNP and PU/GO nanocomposites versus pure PU. Figure 8a presents a quite homogeneous and smooth surface of the pure PU. The incorporation of GNP changes the morphology and grants the nanocomposites a more flake–like morphology. The fractured surface of the PU/GNP nanocomposites with increasing proportions of GNP is seen to have some aggregated GNPs and apparent irregularities compared to the surface of pure

PU, suggesting the poor dispersibility of the individual GNPs (indicated by the red arrows and ellipses) as illustrated in Figure 8b–d [80]. As a result, the SEM morphology can provide a demonstration of the dispersion quality of the GNP within the PU [3,35]. In the other samples of PU/GO, the GO platelets show better attachment to the PU chains, particularly the hard segments, owing to the interfacial adhesion between the GO surfaces and PU chains, and thus a good enhancement of the dispersion of GO in the PU nanocomposites [22,58,73].
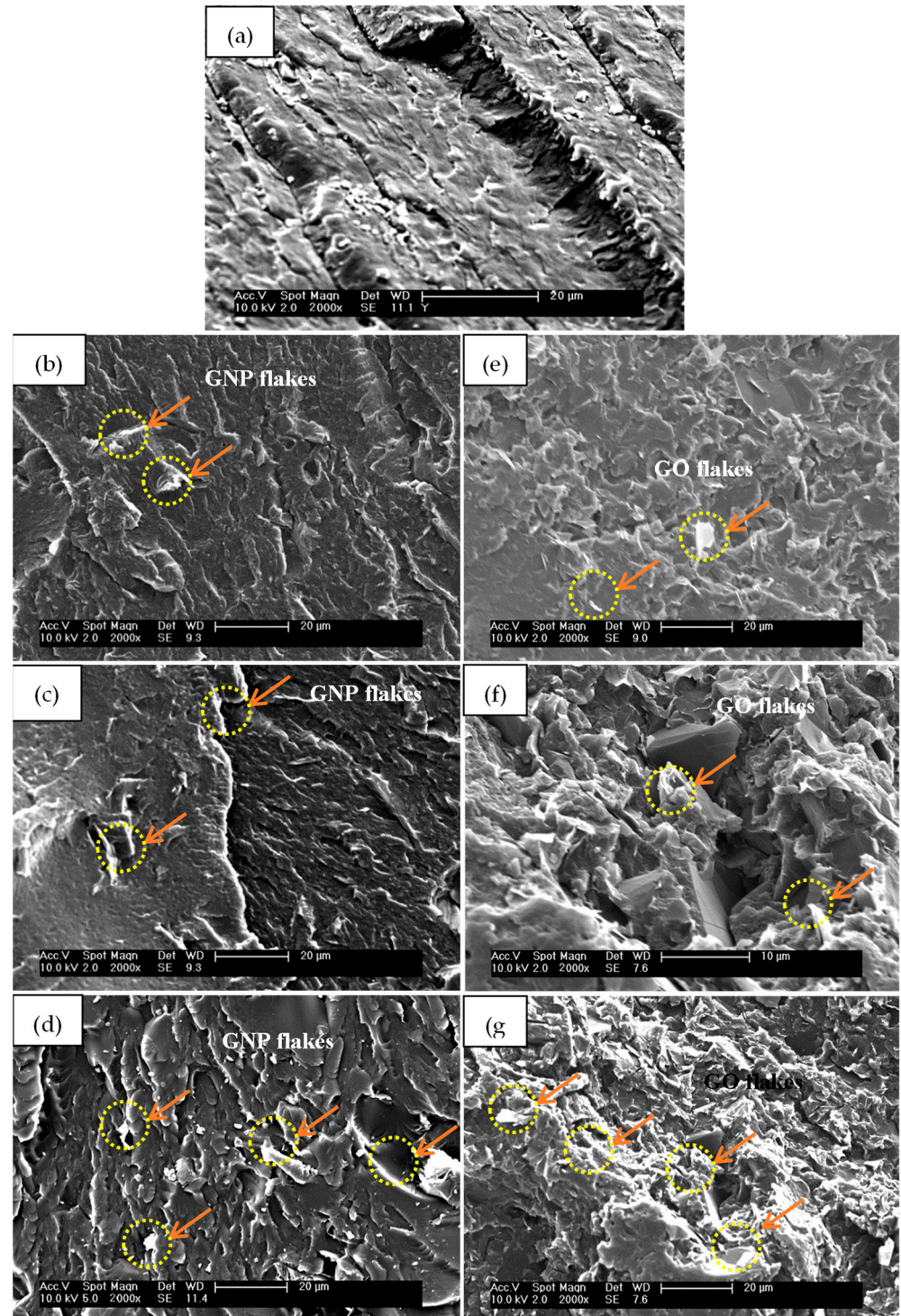

Figure 8. SEM images of cryogenic-fracture surfaces of (**a**) pure PU, (**b**–**d**) PU/GNP, and (**e**–**g**) PU/GO nanocomposites with loadings of GNP and GO of 0.25 wt.%, 0.5 wt.%, and 0.75 wt.%, respectively.

3.5. TEM Results

Figure 9 shows the TEM images, demonstrating the nanoscale dispersion of nanofillers within the PU nanocomposites. The dark areas are regions of GNP; these features may be attributed to the linkage of GNP with the PU matrix. The microtome-cut samples at 0.25%, 0.5 %, and 0.75% GNP show well-dispersed GNPs in the PU matrix at a low loading (0.25%). However, the individual GNP tend to aggregate and increase in thickness with increasing loadings. As a result, this is referred to as a strong interfacial interaction between the GNPs and PU due to a proper dispersion technique with a small amount of reinforcement [81–83]. In the case of the PU/GO nanocomposites, the TEM images exhibit a uniform dispersion and distribution of GO flakes at a minimum concentration. On the contrary, this trend is seen to change as the amount of GO increases within the PU matrix, which is clear evidence for the tendency of GO towards restacking, despite the existence of strong interactions with the PU chains [84–86]. In general, the TEM results show a good agreement with the SEM results regarding the dispersion of GNP and GO within a PU matrix.
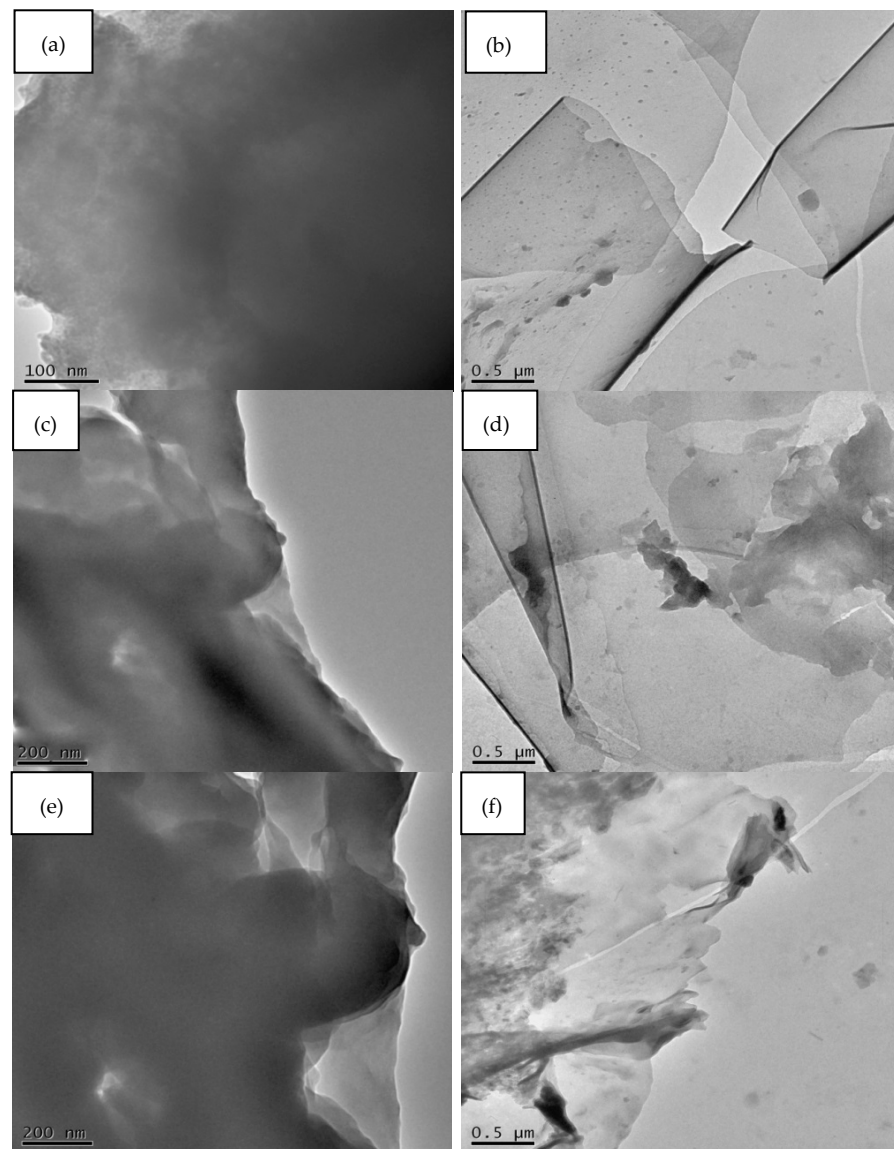

Figure 9. TEM images: (**a**,**c**,**e**) PU/GNP; (**b**,**d**,**f**) PU/GO nanocomposites with loadings of 0.25 wt.%, 0.5 wt.%, and 0.75 wt.%, respectively, with a magnification scale of 200 μm and 0.5 μm.

3.6. Mechanical Performance Results

A comparative study of the mechanical properties of PU nanocomposites with GNPs and GO was conducted. The tensile behaviour of PU when GNP and GO nanofillers were incorporated using in situ polymerisation displayed a good improvement compared to pure PU. These enhancements in tensile properties such as the tensile modulus and yield strength were determined through a stress–strain analysis, as depicted in Figure 10. Based on the overall enhancement of the tensile performance of the PU/GNP and PU/GO nanocomposites, several factors affect the efficiency/quality of tensile improvement, including the GNPs' and GO's dispersion, concentration, and bonding ratio within the PU polymer [6,87–89]. To some extent, Young's modulus has been increased from 214 MPa for PU to maximum values of 320 MPa, 390 MPa, and 490 MPa for GNP loadings of 0.25, 0.5, and 0.75 wt.%, respectively. The increments in the percentage of the maximum modulus were recorded as 50%, 81%, and 127%, respectively. Similarly, the PU/GO nanocomposites have the greatest modulus at percentages of 0.25 and 0.5 wt.% compared to the PU/GNP nanocomposites. The possible reason for this substantial improvement could be related to the superior dispersion and interfacial adhesion between the functional groups on the GO surfaces with a high stiffness and the hard segments of PU, which are observed to increase to 136% and 152% for 0.25 and 0.5 wt.%, respectively [58]. However, this increase is seen to reduce at a 0.75% loading of GO. This is because of the high aspect ratio of GO leading to the clustering of GO at higher concentrations and thus increasing the number of stress concentration sites, which reduce the quality of the resultant nanocomposites through a reduction in stress transfer efficiency [2,90,91].
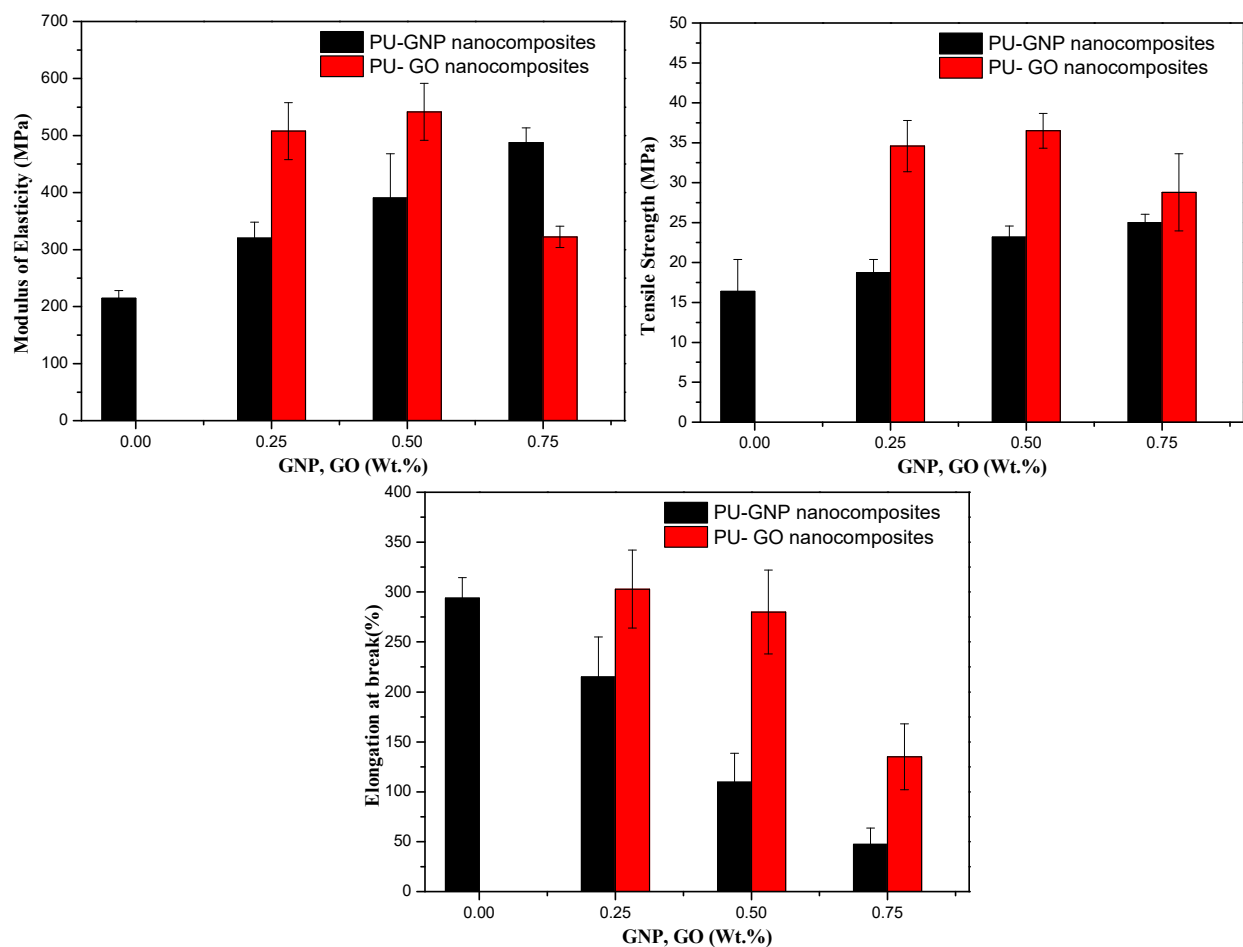

Figure 10. Comparative mechanical properties of the PU/GNP and PU/GO nanocomposites.

The same results are observed regarding the tensile strength at break: all the tensile values have been increased as a function of the nanofillers' addition from 16.3 MPa for pure PU to 18 MPa, 23 MPa, and 25 MPa with GNP loadings of 0.25, 0.5, and 0.75 wt.%, respectively. The effective load transfer is attributed to such an improvement in tensile strength with the assumption of an increase in the microphase separation of PU [6,33,90]. A similar trend is observed for the PU/GO nanocomposites, whose increases are 111 MPa, 123 MPa, and 28 MPa for GO loadings of 0.25, 0.5, and 0.75 wt.%, respectively, compared to that of pure PU. A noticeable improvement in the tensile strength of the PU/GO samples was observed compared to that of PU/GNP; this is likely due to the efficient interfacial interaction, as previously mentioned, along with the modulus' improvement [92].

However, a decrease is observed at a 0.75% loading, suggesting aggregation at a high GO content [89]. The restrictive effect of the GNP/GO nanofillers on the PU chains' mobility results in a decrement in elongation at break for their nanocomposites. Reduction ratios of 27% and 72% were seen for the maximum loadings of GNP and GO, respectively, compared to pure PU. However, an increase at 0.25 of GO with respect to PU in the elongation at break point was also observed, suggesting a form of soft transition or even a lubricating effect between the GO and PU chains, depending on the dispersibility of GO within PU [3,22].

4. Conclusions

This study has successfully synthesised novel PU nanocomposites with two different graphene-based nanofillers (GNP and GO) with a chain extender (1,5 Pentanediol). The authors investigated the effect of the addition of different nano-scale fillers at three different loadings (0.25, 0.5, and 0.75 wt.%) on the mechanical, thermal, and morphological properties of the PU nanocomposites formed via in situ polymerisation. The thermal transitions obtained by DSC showed that the melting temperature (T_m) and crystallisation temperature (T_c) have been enhanced by the addition of GNP at any level. The enthalpies of fusion and crystallisation (ΔH_m and ΔH_C) were also improved, meaning that the nanofillers worked as nucleation agents. This result was obtained because the improved dispersion and interaction of GNP can lead to microphase separation, and thus the better crystallisation of hard segments. In the case of the addition of GO, a similar trend was seen, with an enhanced melting point of the resultant PU nanocomposites due to strong interfacial adhesion between the GO and PU chains.

The WAXS results showed an improvement in the crystalline peak of pure PU with the addition of GNP, while the presence of GO caused the diffraction peak to vanish. This is due to the functional group on the surface of GO leading to interfacial interaction with the PU matrix.

The SAXS results indicate that the presence of GNP and GO particularly stimulated an increase in the microphase separation of the PU matrix. SEM and TEM morphologies were used to support the dispersion quality obtained using different reinforcement nanofillers. The micrographs showed that both GNP and GO dispersed effectively within PU at low levels of concentration and some clusters of aggregation were observed at high concentrations. The mechanical tests showed a dramatic increase in the tensile properties as a result of incorporating GNP and GO nanofillers in comparison with the PU polymer. Thus, the improved modulus of the resultant PU nanocomposites was seen to have a greater value at 0.5 wt.% GNP and GO loadings. However, the tensile strength and elongation at break decreased after this percentage due to the suppression of strain hardening.

Author Contributions: M.A.: methodology; investigation; resources; funding acquisition; writing—review and editing; H.Z.N.: methodology; validation, writing—review and editing; Z.K.A.: formal analysis; J.K.W.: investigation, funding acquisition; A.S.: resources. All authors have read and agreed to the published version of the manuscript.

References

1. Valentini, M.; Piana, F.; Pionteck, J.; Lamastra, F.R.; Nanni, F. Electromagnetic properties and performance of exfoliated graphite (EG)–Thermoplastic polyurethane (TPU) nanocomposites at microwaves. *Compos. Sci. Technol.* **2015**, *114*, 26–33. [CrossRef]
2. Yadav, S.K.; Cho, J.W. Functionalized graphene nanoplatelets for enhanced mechanical and thermal properties of polyurethane nanocomposites. *Appl. Surf. Sci.* **2013**, *266*, 360–367. [CrossRef]
3. Huang, A.; Wang, H.; Ellingham, T.; Peng, X.; Turng, L.-S. An improved technique for dispersion of natural graphite particles in thermoplastic polyurethane by sub-critical gas-assisted processing. *Compos. Sci. Technol.* **2019**, *182*, 107783. [CrossRef]
4. Li, L.; Xu, L.; Ding, W.; Lu, H.; Zhang, C.; Liu, T. Molecular-engineered hybrid carbon nanofillers for thermoplastic polyurethane nanocomposites with high mechanical strength and toughness. *Compos. Part B Eng.* **2019**, *177*, 107381. [CrossRef]
5. Amir Rostam, M.I.M. High-performance thermoplastic polyurethane nanocomposites induced by hybrid application of functionalized graphene and carbon nanotubes. *J. Appl. Polym. Sci.* **2019**, *137*, 48520. [CrossRef]
6. Abrisham, M.; Panahi-Sarmad, M.; Mir Mohamad Sadeghi, G.; Arjmand, M.; Dehghan, P.; Amirkiai, A. Microstructural design for enhanced mechanical property and shape memory behavior of polyurethane nanocomposites: Role of carbon nanotube, montmorillonite, and their hybrid fillers. *Polym. Test.* **2020**, *89*, 106642. [CrossRef]
7. Pokharel, P.; Pant, B.; Pokhrel, K.; Pant, H.R.; Lim, J.-G.; Lee, D.S.; Kim, H.-Y.; Choi, S. Effects of functional groups on the graphene sheet for improving the thermomechanical properties of polyurethane nanocomposites. *Compos. Part B Eng.* **2015**, *78*, 192–201. [CrossRef]
8. Chen, J.; Liu, B.; Gao, X.; Xu, D. A review of the interfacial characteristics of polymer nanocomposites containing carbon nanotubes. *RSC Adv.* **2018**, *8*, 28048–28085. [CrossRef] [PubMed]
9. Prisacariu, C. *Polyurethane Elastomers: From Morphology to Mechanical Aspects*; Springer: Vienna, Austria; New York, NY, USA, 2011.
10. Al-obad, Z.K.M. Designing PU Resins for Fibre Composite Applications. Ph.D. Thesis, University of Manchester, Manchester, UK, 2017.
11. Naji, H.Z.N. Fabricating of Multiscale Composite Materials Based on TPU Reinforced by Carbon Fibre and Graphene Nanoplatelets (GNPs). Ph.D. Thesis, University of Manchester, Manchester, UK, 2019.
12. Albozahid, M.A.M.A. Design of Novel High Modulus TPUs for NanoComposite Applications. Ph.D. Thesis, University of Manchester, Manchester, UK, 2018.
13. Adak, B.; Butola, B.S.; Joshi, M. Effect of organoclay-type and clay-polyurethane interaction chemistry for tuning the morphology, gas barrier and mechanical properties of clay/polyurethane nanocomposites. *Appl. Clay Sci.* **2018**, *161*, 343–353. [CrossRef]
14. Albozahid, M.; Naji, H.Z.; Alobad, Z.K.; Saiani, A. Enhanced mechanical, crystallisation and thermal properties of graphene flake-filled polyurethane nanocomposites: The impact of thermal treatment on the resulting microphase-separated structure. *J. Polym. Res.* **2021**, *28*, 302. [CrossRef]
15. Kim, H.J.; Han, J.; Son, Y. Effect of a Monomer Composition on the Mechanical Properties and Glass Transition Temperature of a Waterborne Polyurethane/Graphene Oxide and Waterborne Polyurethane/MWCNT Nanocomposite. *Polymers* **2020**, *12*, 2013. [CrossRef]
16. Amirkhosravi, M.; Yue, L.; Ju, T.; Manas-Zloczower, I. Designing thermal annealing to control mechanical performance of thermoplastic polyurethane elastomers. *Polymer* **2021**, *214*, 123254. [CrossRef]
17. Tayfun, U.; Kanbur, Y.; Abacı, U.; Güney, H.Y.; Bayramlı, E. Mechanical, electrical, and melt flow properties of polyurethane elastomer/surface-modified carbon nanotube composites. *J. Compos. Mater.* **2016**, *51*, 1987–1996. [CrossRef]
18. Bera, M.; Maji, P.K. Effect of structural disparity of graphene-based materials on thermo-mechanical and surface properties of thermoplastic polyurethane nanocomposites. *Polymer* **2017**, *119*, 118–133. [CrossRef]
19. Stankovich, S.; Dikin, D.A.; Dommett, G.H.; Kohlhaas, K.M.; Zimney, E.J.; Stach, E.A.; Piner, R.D.; Nguyen, S.T.; Ruoff, R.S. Graphene-based composite materials. *Nature* **2006**, *442*, 282–286. [CrossRef]

20. Wychowaniec, J.K.; Iliut, M.; Borek, B.; Muryn, C.; Mykhaylyk, O.O.; Edmondson, S.; Vijayaraghavan, A. Elastic flow instabilities and macroscopic textures in graphene oxide lyotropic liquid crystals. *NPJ 2D Mater. Appl.* **2021**, *5*, 11. [CrossRef]

21. Albozahid, M.; Habeeb, S.A.; Ismael Alhilo, N.A.; Saiani, A. The impact of graphene nanofiller loading on the morphology and rheology behaviour of highly rigid polyurethane copolymer. *Mater. Res. Express* **2020**, *7*, 125304. [CrossRef]

22. Tang, X.-Z.; Mu, C.; Zhu, W.; Yan, X.; Hu, X.; Yang, J. Flexible polyurethane composites prepared by incorporation of polyethylenimine-modified slightly reduced graphene oxide. *Carbon* **2016**, *98*, 432–440. [CrossRef]

23. Henning Döscher, T.S.; Neef, C.; Thielmann, A.; Reiss, T. Graphene Roadmap Briefs (No. 2): Industrialization status and prospects 2020. *2D Mater.* **2021**, *8*. [CrossRef]

24. Sang, G.; Dong, J.; He, X.; Jiang, J.; Li, J.; Xu, P.; Ding, Y. Electromagnetic interference shielding performance of polyurethane composites: A comparative study of GNs-IL/Fe3O4 and MWCNTs-IL/Fe3O4 hybrid fillers. *Compos. Part B Eng.* **2019**, *164*, 467–475. [CrossRef]

25. Yin, C.; Du, Z.; Wen, S.; Wang, J. High performance of reduced sulfonated graphite oxide nanoplatelets/polyurethane composites. *Mater. Lett.* **2016**, *168*, 20–23. [CrossRef]

26. Pokharel, P.; Lee, D.S. High performance polyurethane nanocomposite films prepared from a masterbatch of graphene oxide in polyether polyol. *Chem. Eng. J.* **2014**, *253*, 356–365. [CrossRef]

27. Lee, S.H.; Oh, C.R.; Lee, D.S. Large Improvement in the Mechanical Properties of Polyurethane Nanocomposites Based on a Highly Concentrated Graphite Nanoplate/Polyol Masterbatch. *Nanomaterials* **2019**, *9*, 389. [CrossRef]

28. Potts, J.R.; Dreyer, D.R.; Bielawski, C.W.; Ruoff, R.S. Graphene-based polymer nanocomposites. *Polymer* **2011**, *52*, 5–25. [CrossRef]

29. Chandrasekaran, S.; Seidel, C.; Schulte, K. Preparation and characterization of graphite nano-platelet (GNP)/epoxy nano-composite: Mechanical, electrical and thermal properties. *Eur. Polym. J.* **2013**, *49*, 3878–3888. [CrossRef]

30. Hoepfner, J.C.; Loos, M.R.; Pezzin, S.H. Evaluation of thermomechanical properties of polyvinyl butyral nanocomposites reinforced with graphene nanoplatelets synthesized by in situ polymerization. *J. Appl. Polym. Sci.* **2018**, *135*, 46157. [CrossRef]

31. Jayadurga Iyer Ganapathi, D.M.K.; Frank, T. Fisher. Effect of multistage sonication on dispersive mixing of polymer nanocomposites characterized via shear-induced crystallization behavior. *J. Appl. Polym. Sci* **2017**, *134*, 44681. [CrossRef]

32. Khoshsefat, M.; Ahmadjo, S.; Mortazavi, S.M.M.; Zohuri, G.H. Reinforcement effects of nanocarbons on catalyst behaviour and polyethylene properties through in situ polymerization. *RSC Adv.* **2016**, *6*, 88625–88632. [CrossRef]

33. Bernard, C.; Goodwin, D.G., Jr.; Gu, X.; Celina, M.; Nyden, M.; Jacobs, D.; Sung, L.; Nguyen, T. Graphene oxide/waterborne polyurethane nanocoatings: Effects of graphene oxide content on performance properties. *J. Coat. Technol. Res.* **2020**, *17*, 255–269. [CrossRef]

34. Liu, S.; Tian, M.; Yan, B.; Yao, Y.; Zhang, L.; Nishi, T.; Ning, N. High performance dielectric elastomers by partially reduced graphene oxide and disruption of hydrogen bonding of polyurethanes. *Polymer* **2015**, *56*, 375–384. [CrossRef]

35. Song, H.W.M.; Yanfei, W.; Yadong, Z.; Ahmad, U.; Zhanhu, G. Waterborne Polyurethane/Graphene Oxide Nanocomposites with Enhanced Properties. *Sci. Adv. Mater.* **2017**, *9*, 705–714. [CrossRef]

36. Luan, Y.; Gao, F.; Li, Y.; Yang, J.; Hu, Y.; Guo, Z.; Wang, Z.; Zhou, A. Healing mechanisms induced by synergy of Graphene-CNTs and microwave focusing effect for the thermoplastic polyurethane composites. *Compos. Part A Appl. Sci. Manuf.* **2018**, *106*, 34–41. [CrossRef]

37. Jun, Y.-s.; Habibpour, S.; Hamidinejad, M.; Park, M.G.; Ahn, W.; Yu, A.; Park, C.B. Enhanced electrical and mechanical properties of graphene nano-ribbon/thermoplastic polyurethane composites. *Carbon* **2021**, *174*, 305–316. [CrossRef]

38. Lawal, A.T. Graphene-based nano composites and their applications. A review. *Biosens. Bioelectron.* **2019**, *141*, 111384. [CrossRef] [PubMed]

39. Rourke, J.P.; Pandey, P.A.; Moore, J.J.; Bates, M.; Kinloch, I.A.; Young, R.J.; Wilson, N.R. *The Real Graphene Oxide Revealed: Stripping the Oxidative Debris from the Graphene-Like Sheets*; Wiley-VCH: Weinheim, Germany, 2011.

40. Muayad Albozahid, H.N.; Alobad, Z.; Saiani, A. Effect of Dispersion Methods on The Performance of Novel Rigid Copolymer Polyurethane Nanocomposites Based on Graphene Nanofillers. *Polym.-Plast. Technol. Mater.* **2021**, *60*, 16. [CrossRef]

41. Cho, E.-C.; Huang, J.-H.; Li, C.-P.; Chang-Jian, C.-W.; Lee, K.-C.; Hsiao, Y.-S.; Huang, J.-H. Graphene-based thermoplastic composites and their application for LED thermal management. *Carbon* **2016**, *102*, 66–73. [CrossRef]

42. McAllister, M.J.; Li, J.; Adamson, D.H.; Schniepp, H.C.; Abdala, A.A.; Liu, J.; Herrera-Alonso, M.; Milius, D.L.; Car, R.; Prud'homme, R.K.; et al. Single Sheet Functionalized Graphene by Oxidation and Thermal Expansion of Graphite. *Chem. Mater* **2007**, *19*, 4396–4404. [CrossRef]

43. Pashupati Pokharel, H.B.; Lim, J.; Lee, K.Y.; Choi, S. Effects of titanate treatment on morphology and mechanical properties of graphene nanoplatelets/high density polyethylene nanocomposites. *J. Appl. Polym. Sci.* **2015**, *132*, 42073. [CrossRef]

44. Lin, J.; Zhang, H.; Tang, M.; Tu, W.; Zhang, X. Improved Thermal Property of a Multilayered Graphite Nanoplatelets Filled Silicone Resin Composite. *J. Mater. Eng. Perform.* **2014**, *24*, 920–929. [CrossRef]

45. Li, Y.C.; Tjong, S.C.; Li, R.K.Y. Electrical conductivity and dielectric response of poly(vinylidene fluoride)–graphite nanoplatelet composites. *Synth. Met.* **2010**, *160*, 1912–1919. [CrossRef]

46. Siburian, R.; Sari, D.R.; Gultom, J.; Sihotang, H.; Raja, S.L.; Gultom, J.; Supeno, M. Performance of graphite and graphene as electrodes in primary cell battery. *J. Phys. Conf. Ser.* **2018**, *1116*, 042034. [CrossRef]

47. Mohd Zaid, N.A.; Idris, N.H. Enhanced Capacitance of Hybrid Layered Graphene/Nickel Nanocomposite for Supercapacitors. *Sci. Rep.* **2016**, *6*, 32082. [CrossRef] [PubMed]

48. Filip, D.; Macocinschi, D.; Vlad, S. Thermogravimetric study for polyurethane materials for biomedical applications. *Compos. Part B Eng.* **2011**, *42*, 1474–1479. [CrossRef]

49. Alobad, Z.K.; Albozahid, M.; Naji, H.Z.; Alraheem, H.S.; Saiani, A. Influence of hard segments content on thermal, morphological and mechanical properties of homo and co-polyurethanes: A comparative study. *Arch. Mater. Sci. Eng.* **2021**, *1*, 5–16. [CrossRef]

50. Mahapatra, S.S.; Yadav, S.K.; Yoo, H.J.; Ramasamy, M.S.; Cho, J.W. Tailored and strong electro-responsive shape memory actuation in carbon nanotube-reinforced hyperbranched polyurethane composites. *Sens. Actuators B Chem.* **2014**, *193*, 384–390. [CrossRef]

51. Valentini, L.; Cardinali, M.; Kenny, J. Hot press transferring of graphene nanoplatelets on polyurethane block copolymers film for electroactive shape memory devices. *J. Polym. Sci. Part B Polym. Phys.* **2014**, *52*, 1100–1106. [CrossRef]

52. Tounici, A.; Martín-Martínez, J.M. Addition of small amounts of graphene oxide in the polyol during the synthesis of waterborne polyurethane urea adhesives for improving their adhesion properties. *Int. J. Adhes. Adhes.* **2021**, *104*, 102725. [CrossRef]

53. Anandhan, S.; Lee, H.S. Influence of organically modified clay mineral on domain structure and properties of segmented thermoplastic polyurethane elastomer. *J. Elastomers Plast.* **2012**, *46*, 217–232. [CrossRef]

54. Habibpour, S.; Um, J.G.; Jun, Y.-S.; Bhargava, P.; Park, C.B.; Yu, A. Structural Impact of Graphene Nanoribbon on Mechanical Properties and Anti-corrosion Performance of Polyurethane Nanocomposites. *Chem. Eng. J.* **2021**, *405*, 126858. [CrossRef]

55. Harb, S.V.; Pulcinelli, S.H.; Santilli, C.V.; Knowles, K.M.; Hammer, P. A Comparative Study on Graphene Oxide and Carbon Nanotube Reinforcement of PMMA-Siloxane-Silica Anticorrosive Coatings. *ACS Appl. Mater. Interfaces* **2016**, *8*, 16339–16350. [CrossRef]

56. Pandey, S.; Jana, K.K.; Aswal, V.K.; Rana, D.; Maiti, P. Effect of nanoparticle on the mechanical and gas barrier properties of thermoplastic polyurethane. *Appl. Clay Sci.* **2017**, *146*, 468–474. [CrossRef]

57. Muayad Albozahid, H.Z.N.; Alobad, Z.K.; Wychowaniec, J.K.; Saiani, A. Synthesis and Characterisation of Hard Copolymer Polyurethane/Functionalised Graphene Nanocomposites: Investigation of Morphology, Thermal Stability and Rheological Properties. *J. Appl. Polym. Sci.* **2022**. [CrossRef]

58. Bian, J.; Lin, H.L.; He, F.X.; Wei, X.W.; Chang, I.T.; Sancaktar, E. Fabrication of microwave exfoliated graphite oxide reinforced thermoplastic polyurethane nanocomposites: Effects of filler on morphology, mechanical, thermal and conductive properties. *Compos. Part A Appl. Sci. Manuf.* **2013**, *47*, 72–82. [CrossRef]

59. Lei, H.; Liu, Z.; He, C.; Zhang, S.-C.; Liu, Y.-Q.; Hua, C.-J.; Li, X.-M.; Li, F.; Chen, C.-M.; Cai, R. Graphene enhanced low-density polyethylene by pretreatment and melt compounding. *RSC Adv.* **2016**, *6*, 101492–101500. [CrossRef]

60. Nguyen, D.A.; Lee, Y.R.; Raghu, A.V.; Jeong, H.M.; Shin, C.M.; Kim, B.K. Morphological and physical properties of a thermoplastic polyurethane reinforced with functionalized graphene sheet. *Polym. Int.* **2009**, *58*, 412–417. [CrossRef]

61. Albozahid, M.; Naji, H.Z.; Alobad, Z.K.; Saiani, A. Effect of OMMT reinforcement on morphology and rheology properties of polyurethane copolymer nanocomposites. *J. Elastomers Plast.* **2021**. [CrossRef]

62. Roy, S.; Srivastava, S.K.; Pionteck, J.; Mittal, V. Mechanically and Thermally Enhanced Multiwalled Carbon Nanotube-Graphene Hybrid filled Thermoplastic Polyurethane Nanocomposites. *Macromol. Mater. Eng.* **2015**, *300*, 346–357. [CrossRef]

63. Lee, M.; Koo, J.; Ki, H.; Lee, K.H.; Min, B.H.; Lee, Y.C.; Kim, J.H. Phase separation and electrical conductivity of nanocomposites made of ether-/ester-based polyurethane blends and carbon nanotubes. *Macromol. Res.* **2017**, *25*, 231–242. [CrossRef]

64. Raftopoulos, K.N.; Janowski, B.; Apekis, L.; Pielichowski, K.; Pissis, P. Molecular mobility and crystallinity in polytetramethylene ether glycol in the bulk and as soft component in polyurethanes. *Eur. Polym. J.* **2011**, *47*, 2120–2133. [CrossRef]

65. Chung, Y.-C.; Khiem, N.D.; Chun, B.C. Characterization of a polyurethane copolymer covalently linked to graphite and the influence of graphite on electric conductivity. *J. Compos. Mater.* **2014**, *49*, 1689–1703. [CrossRef]

66. Thakur, S.; Karak, N. Ultratough, Ductile, Castor Oil-Based, Hyperbranched, Polyurethane Nanocomposite Using Functionalized Reduced Graphene Oxide. *ACS Sustain. Chem. Eng.* **2014**, *2*, 1195–1202. [CrossRef]

67. Jofre-Reche, J.A.; García-Pacios, V.; Costa, V.; Colera, M.; Martín-Martínez, J.M. Role of the interactions between carbonate groups on the phase separation and properties of waterborne polyurethane dispersions prepared with copolymers of polycarbonate diol. *Prog. Org. Coat.* **2015**, *88*, 199–211. [CrossRef]

68. Idumah, C.I.; Hassan, A. Hibiscus Cannabinus Fiber/PP based Nano-Biocomposites Reinforced with Graphene Nanoplatelets. *J. Nat. Fibers* **2017**, *14*, 691–706. [CrossRef]

69. Yang, D.; Xu, H.; Yu, W.; Wang, J.; Gong, X. Dielectric properties and thermal conductivity of graphene nanoplatelet filled poly(vinylidene fluoride) (PVDF)/poly(methyl methacrylate) (PMMA) blend. *J. Mater. Sci. Mater. Electron.* **2017**, *28*, 13006–13012. [CrossRef]

70. Thakur, S.; Karak, N. One-step approach to prepare magnetic iron oxide/reduced graphene oxide nanohybrid for efficient organic and inorganic pollutants removal. *Mater. Chem. Phys.* **2014**, *144*, 425–432. [CrossRef]

71. Albozahid, M.; Naji, H.Z.; Alobad, Z.K.; Saiani, A. TPU nanocomposites tailored by graphene nanoplatelets: The investigation of dispersion approaches and annealing treatment on thermal and mechanical properties. *Polym. Bull.* **2021**, *79*, 8269–8307. [CrossRef]

72. Strankowski, M. Effect of Variation of Hard Segment Content and Graphene-Based Nanofiller Concentration on Morphological, Thermal, and Mechanical Properties of Polyurethane Nanocomposites. *Int. J. Polym. Sci.* **2018**, *2018*, 1090753. [CrossRef]

73. Pokharel, P.; Lee, S.H.; Lee, D.S. Thermal, Mechanical, and Electrical Properties of Graphene Nanoplatelet/Graphene Oxide/Polyurethane Hybrid Nanocomposite. *J. Nanosci. Nanotechnol.* **2015**, *15*, 211–214. [CrossRef]

74. Saiani, A.; Rochas, C.; Eeckhaut, G.; Daunch, W.A.; Leenslag, J.W.; Higgins, J.S. Origin of Multiple Melting Endotherms in a High Hard Block Content Polyurethane. 2. Structural Investigation. *Macromolecules* **2004**, *37*, 1411–1421. [CrossRef]

75. Saiani, A.; Novak, A.; Rodier, L.; Eeckhaut, G.; Leenslag, J.-W.; Higgins, J.S. Origin of Multiple Melting Endotherms in a High Hard Block Content Polyurethane: Effect of Annealing Temperature. *Macromolecules* **2007**, *40*, 7252–7262. [CrossRef]

76. Kong, Z.; Tian, Q.; Zhang, R.; Yin, J.; Shi, L.; Ying, W.B.; Hu, H.; Yao, C.; Wang, K.; Zhu, J. Reexamination of the microphase separation in MDI and PTMG based polyurethane: Fast and continuous association/dissociation processes of hydrogen bonding. *Polymer* **2019**, *185*, 121943. [CrossRef]

77. Hosseini-Sianaki, T.; Nazockdast, H.; Salehnia, B.; Nazockdast, E. Microphase separation and hard domain assembly in thermoplastic polyurethane/multiwalled carbon nanotube nanocomposites. *Polym. Eng. Sci.* **2015**, *55*, 2163–2173. [CrossRef]

78. Skosana, S.J.; Khoathane, C.; Malwela, T. Enhancing the adhesion strength of polyurethane coatings by dispersing layered silicates via sonication and high-shear mixing method. *Polym. Bull.* **2020**, *78*, 203–221. [CrossRef]

79. Tarasov, A.E.; Anokhin, D.V.; Propad, Y.V.; Bersenev, E.A.; Razorenov, S.V.; Garkushin, G.V.; Badamshina, E.R. Synergetic effect of fullerene and graphene oxide nanoparticles on mechanical characteristics of cross-linked polyurethanes under static and dynamic loading. *J. Compos. Mater.* **2019**, *53*, 3797–3805. [CrossRef]

80. Muayad Albozahid, H.Z.N.; Alobad, Z.K.; Saiani, A. Study on the effect of tailoring the hard copolymer polyurethane on the thermal, mechanical and electrical properties of hard copolymer polyurethane/multi-walled carbon nanotubes nanocomposites. *J. Compos. Mater.* **2022**, *56*, 1467–1480. [CrossRef]

81. Cai, D.; Jin, J.; Yusoh, K.; Rafiq, R.; Song, M. High performance polyurethane/functionalized graphene nanocomposites with improved mechanical and thermal properties. *Compos. Sci. Technol.* **2012**, *72*, 702–707. [CrossRef]

82. Lin, J.; Zhang, P.; Zheng, C.; Wu, X.; Mao, T.; Zhu, M.; Wang, H.; Feng, D.; Qian, S.; Cai, X. Reduced silanized graphene oxide/epoxy-polyurethane composites with enhanced thermal and mechanical properties. *Appl. Surf. Sci.* **2014**, *316*, 114–123. [CrossRef]

83. Lee, Y.R.; Raghu, A.V.; Jeong, H.M.; Kim, B.K. Properties of Waterborne Polyurethane/Functionalized Graphene Sheet Nanocomposites Prepared by an in situ Method. *Macromol. Chem. Phys.* **2009**, *210*, 1247–1254. [CrossRef]

84. Chieng, B.; Ibrahim, N.; Yunus, W.; Hussein, M.; Then, Y.; Loo, Y. Effects of Graphene Nanoplatelets and Reduced Graphene Oxide on Poly(lactic acid) and Plasticized Poly(lactic acid): A Comparative Study. *Polymers* **2014**, *6*, 2232–2246. [CrossRef]

85. Liu, Y.; Zhang, Y.; Duan, L.; Zhang, W.; Su, M.; Sun, Z.; He, P. Polystyrene/graphene oxide nanocomposites synthesized via Pickering polymerization. *Prog. Org. Coat.* **2016**, *99*, 23–31. [CrossRef]

86. Albozahid, M.; Naji, H.; Alobad, Z.; Saiani, A. The effect of OMMT reinforcement and annealing treatment on mechanical and thermal properties of Polyurethane Copolymer nanocomposites. *J. Elastomers Plast.* **2021**, *54*, 477–493. [CrossRef]

87. Pokharel, P.; Choi, S.; Lee, D.S. The effect of hard segment length on the thermal and mechanical properties of polyurethane/graphene oxide nanocomposites. *Compos. Part A Appl. Sci. Manuf.* **2015**, *69*, 168–177. [CrossRef]

88. Wang, Z.; Li, S.; Wu, Z. The fabrication and properties of a graphite nanosheet/polystyrene composite based on graphite nanosheets treated with supercritical water. *Compos. Sci. Technol.* **2015**, *112*, 50–57. [CrossRef]

89. Lan, Y.; Liu, H.; Cao, X.; Zhao, S.; Dai, K.; Yan, X.; Zheng, G.; Liu, C.; Shen, C.; Guo, Z. Electrically conductive thermoplastic polyurethane/polypropylene nanocomposites with selectively distributed graphene. *Polymer* **2016**, *97*, 11–19. [CrossRef]

90. Li, J.W.; Tsen, W.C.; Tsou, C.H.; Suen, M.C.; Chiu, C.W. Synthetic Environmentally Friendly Castor Oil Based-Polyurethane with Carbon Black as a Microphase Separation Promoter. *Polymers* **2019**, *11*, 1333. [CrossRef]

91. Lei, L.; Xia, Z.; Zhang, L.; Zhang, Y.; Zhong, L. Preparation and properties of amino-functional reduced graphene oxide/waterborne polyurethane hybrid emulsions. *Prog. Org. Coat.* **2016**, *97*, 19–27. [CrossRef]

92. Jiang, S.; Li, Q.; Wang, J.; He, Z.; Zhao, Y.; Kang, M. Multiscale graphene oxide–carbon fiber reinforcements for advanced polyurethane composites. *Compos. Part A Appl. Sci. Manuf.* **2016**, *87*, 1–9. [CrossRef]